RESEARCH ARTICLE



WILEY

Ensemble forecasting of the Zika space-time spread with topological data analysis

Marwah Soliman¹ | Vyacheslav Lyubchich² | Yulia R. Gel¹

¹Department of Mathematical Sciences, University of Texas at Dallas, Richardson Texas

²Chesapeake Biological Laboratory, University of Maryland Center for Environmental Science, Solomons Maryland

Correspondence

Yulia R. Gel, Department of Mathematical Sciences, University of Texas at Dallas, 800 West Campbell Road, Richardson, TX 75080, USA.

Email: ygl@utdallas.edu

Funding information

NSF DMS, Grant/Award Number: 1925346

Summary

As per the records of the World Health Organization, the first formally reported incidence of Zika virus occurred in Brazil in May 2015. The disease then rapidly spread to other countries in Americas and East Asia, affecting more than 1,000,000 people. Zika virus is primarily transmitted through bites of infected mosquitoes of the species Aedes (Aedes aegypti and Aedes albopictus). The abundance of mosquitoes and, as a result, the prevalence of Zika virus infections are common in areas which have high precipitation, high temperature, and high population density. Nonlinear spatio-temporal dependency of such data and lack of historical public health records make prediction of the virus spread particularly challenging. In this article, we enhance Zika forecasting by introducing the concepts of topological data analysis and, specifically, persistent homology of atmospheric variables, into the virus spread modeling. The topological summaries allow for capturing higher order dependencies among atmospheric variables that otherwise might be unassessable via conventional spatio-temporal modeling approaches based on geographical proximity assessed via Euclidean distance. We introduce a new concept of cumulative Betti numbers and then integrate the cumulative Betti numbers as topological descriptors into three predictive machine learning models: random forest, generalized boosted regression, and deep neural network. Furthermore, to better quantify for various sources of uncertainties, we combine the resulting individual model forecasts into an ensemble of the Zika spread predictions using Bayesian model averaging. The proposed methodology is illustrated in application to forecasting of the Zika space-time spread in Brazil in the year 2018.

KEYWORDS

Bayesian model averaging, epidemics, machine learning, neural network, Zika virus

1 | INTRODUCTION

The Zika virus is a flavivirus belonging to the *Flaviviridae* family which also includes yellow fever, dengue, Japanese encephalitis, and West Nile viruses (Goeijenbier et al., 2016). The earliest known occurrence of Zika was identification of the virus in the serum of a rhesus monkey in 1947 in Uganda (Dick, 1952; Dick, Kitchen, & Haddow, 1952). In 2015 Zika virus was detected in Brazil, with an estimate of 1.3 million infection cases, and rapidly was transmitted to other countries

in North and South Americas, as well as East Asia (Heukelbach, Alencar, Kelvin, de Oliveira, & de Góes Cavalcanti, 2016; Malone et al., 2016). Symptoms of Zika virus infection among humans include headache, fever, reddened eyes, rashes, muscle and joint pain. Furthermore, Zika virus can cause severe birth defects when transmitted from a pregnant woman to her fetus. Given a rapid spread of the infection, the World Health Organization declared Zika an epidemic disease from 2015 to 2016 (WHO, 2019).

Zika is primarily transmitted through the bite of infected *Aedes aegypti* and *Aedes albopictus* (CDC, 2018). As a result, the spreading of Zika virus is significantly accelerated by weather conditions favoring the abundance of the Aedes mosquitoes, for example, in temperate climate zones with high humidity and rainfall (Muñoz et al., 2017; Rees, Petukhova, Mascarenhas, Pelcat, & Ogden, 2018; Tjaden, Thomas, Fischer, & Beierkuhnlein, 2013). In addition, the virus can be transmitted from mother to her fetus, also via sexual contacts, blood transfusion, and organ transplantation (WHO, 2019).

Modeling and forecasting Zika spread continues to attract an ever increasing attention, and there exist three general methodological directions rooted in mathematics, statistics, and machine learning (Ferraris, Yssel, & Missé, 2019). Mathematical approaches include vector-borne compartmental and mechanistic transmission models (see, e.g., overviews by Manore & Hyman, 2016; Caminade et al., 2017; Suparit, Wiratsudakul, & Modchang, 2018, and references therein). In turn, statistical methods tend to be largely based on the Box–Jenkins family of models with various exogenous predictors, such as atmospheric variables and data from HealthMap digital surveillance system, Google trends, and Twitter microblogs (see, e.g., McGough, Brownstein, Hawkins, & Santillana, 2017; Teng et al., 2017; Castro, Han, Carvalho, Victora, & França, 2018, and references therein). Finally, machine learning approaches to modeling spread of Zika virus include random forest (RF), boosted regression (BR), and deep feed-forward neural network (DFFN) models (Seo, Lee, & Kim, 2018; Soliman, Lyubchich, & Gel, 2019). As recently shown by Soliman et al. (2019), the DFFN models tend to deliver more competitive predictive performance than RF and BR. Remarkably, while spatio-temporal epidemiology of (re)emerging infectious diseases has been extensively studied in the environmetrics community before (see, for instance, Nobre, Schmidt, & Lopes, 2005; Loh, 2011; Self et al., 2018, and references therein) and despite the increasing popularity of DL tools (McDermott & Wikle, 2019) in the spatio-temporal environmetrics applications, utility of DL approaches in infectious epidemiology remains largely unexplored.

Furthermore, in this article we bring the tools of topological data analysis (TDA) to spatio-temporal modeling (Diggle, Rowlingson, & Tl, 2005; Jang, Lee, Lawson, & Browne, 2007; Nobre et al., 2005; Torabi, 2013; Ugarte, Goicoa, Ibanez, & Militino, 2009) and prediction of the Zika spread. TDA is an emerging methodology at the interface of computational topology, statistics, and machine learning that aims to enhance our understanding on the role of the underlying data shape in dynamics of the data generating process—in our case, the spatio-temporal process of the Zika spread which exhibits a complex nonstationary dependence structure. Since areas with higher quantities of rainfall are principally associated with greater abundance of mosquitoes transmitting Zika (Muñoz et al., 2017), our key idea is to employ TDA to explore the structure and to extract information about the shape of the temperature and precipitation data that may be useful for predicting the spread of Zika infection.

While TDA is found to exhibit high utility in many fields, from genetics to finance to power systems (Gidea & Katz, 2018; Li, Ofori-Boateng, Gel, & Zhang, 2020; Saggar et al., 2018), application of TDA within epidemiology (Costa & Škraba, 2014; Lo & Park, 2018) and even more generally environmetrics (Islambekov & Gel, 2019; Islambekov, Yuvaraj, & Gel, 2019) still remains very limited. In particular, TDA and, specifically, persistent homology (PH) have been employed by Costa & Škraba (2014) for analysis of influenza-like illness during the 2008–2013 flu seasons in Portugal and Italy. Most recently, Lo & Park (2018) show explanatory power of TDA for analysis of Zika spread. Particularly, Lo & Park (2018) use PH factors of the *A. aegypti* mosquito occurrence locations as regressors within a linear model and show a high utility of topological features within a spatial cross-validation framework. The findings of Lo & Park (2018) demonstrate that the model with topological features as regressors yields higher coefficient of determination (*R*²) and lower cross-validation mean squared error than the benchmark linear model without TDA features.

Our method advances the approach of Lo & Park (2018) in multiple ways. By contrast to Lo & Park (2018), who do not consider prediction of Zika incidences over time, our goal is to assess utility of TDA in forecasting *future* spread of Zika, which is the key toward the outbreak emergency preparedness and response. Since mosquito occurrence locations may vary over time, any Zika prediction model based on topological features of mosquito locations also requires forecasts of the mosquito occurrences. Such forecasts are not readily available and may be highly nontrivial, especially in areas with heterogeneous landscapes as Brazil.

By contrast to Lo & Park (2018), we consider TDA in application to shape analysis of temperature and precipitation rather than mosquito data. Such approach allows us to systematically incorporate the future weather and climate forecasts from national weather services and derived topological features of such forecasts into Zika prediction models.

Furthermore, we evaluate predictive utility of TDA based on multiple statistical and machine learning models, such as RF, generalized BR, and DFFN. We introduce a new topological summary concept *cumulative Betti number*, which is used as a predictor of future Zika dynamics and found to deliver a more stable performance than conventional topological characteristics.

Finally, to quantify multiple sources of uncertainty, we develop an adaptive ensemble of Zika forecasting models using Bayesian model averaging (BMA). We illustrate our proposed methodology in application to predicting Zika virus spread for all the 26 states of Brazil during the year 2018.

The key contributions of our article can be summarized as follows:

- To the best of our knowledge, this is the first article introducing topological data features as *predictors of future* space-time spread of infectious diseases.
- To increase stability of the topological summaries and associated derived forecasts, especially under the scenarios with limited sample sizes as in the case of many emerging climate-sensitive infectious diseases, we introduce the notion of *cumulative Betti numbers*. The proposed cumulative Betti numbers can be used in many other applications, beyond infectious epidemiology, which involve noisy data of moderate sample sizes, for example, household travel networks and microgrids.
- We validate utility of our proposed predictive approach across various nonparametric machine learning models, including deep neural networks, which allows for more systematic and objective assessment of predictive gains (if any) delivered by the proposed topological descriptors.

The remainder of the article is organized in four major sections: data description, methodology for epidemiological forecasting and validation metrics, results, and discussion. In Section 2, we provide information on the collected Zika rate, population density, and atmospheric data. We introduce our TDA in Section 3.1 and statistical and machine learning forecasting methodology in Section 3.2. Section 3.3 lists the validation metrics, Section 4 is devoted to validation of the proposed modeling approaches to prediction of Zika rate in Brazil. Finally, the article is concluded with a discussion in Section 5.

2 | DATA DESCRIPTION

Brazil's Ministry of Health publishes cumulative Zika rate on a weekly basis. However, as with many other vector-borne diseases, the official surveillance records for Zika are often incomplete and noisy. For instance, for the year of 2018 the percentage of missing weeks is 28.8%, or 15 weeks out of 52 weeks. In turn, 24 weeks out of 52 weeks are missing in the year of 2017, which is 46.15%. Hence, we analyze monthly records of Zika virus rate per 100,000 individuals, constructed from the cumulative weekly Zika rates published by Brazil's Ministry of Health (MHB, 2018), in each of the 26 states of Brazil and each month during 2017 and 2018.

Considering the strong association between Zika virus transmission and local environmental conditions (e.g., see Tjaden et al., 2013; Muñoz et al., 2017; Rees et al., 2018), we also collected data for precipitation and air temperature. The weather station data are accessed for all states for years 2017 and 2018 (World-Weather-Online, 2018). The forecasted precipitation data for 2018 are obtained from INMET (2019). To ensure consistency in temporal resolutions of Zika and atmospheric data, all daily atmospheric variables are aggregated to a monthly scale.

3 | METHODOLOGY FOR EPIDEMIOLOGICAL FORECASTING

3.1 | Topological data analysis

TDA is a rapidly emerging methodology at the interface of computational topology, statistics, and machine learning which allows for a systematic multilens assessment of the underlying topology and geometry of the data generating process (Carlsson, 2009; Chazal & Michel, 2017; Zomorodian & Carlsson, 2005). In this article, we primarily employ tools of PH within the TDA framework. The ultimate idea of PH is to quantify dynamics of topological properties exhibited by the data that live in Euclidean or abstract metric space, at various resolution scales. The PH approach is implemented in the two key steps: first, the underlying hidden topology of the observed dataset is approximated using certain

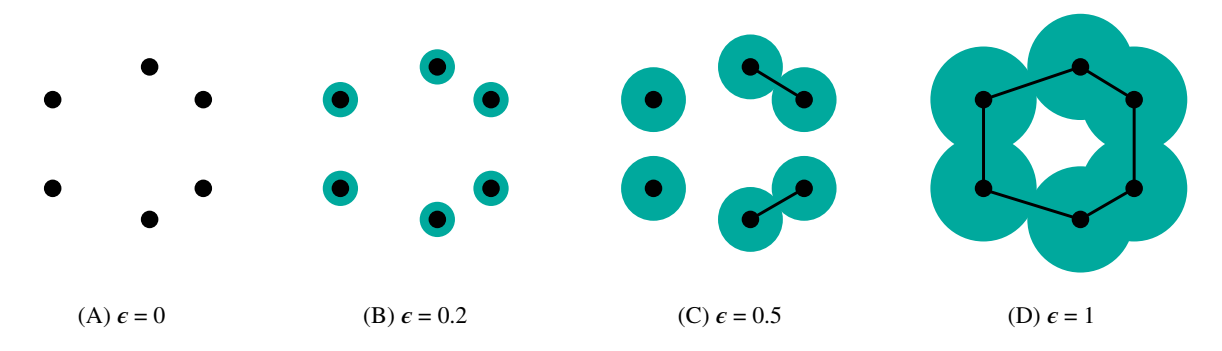


FIGURE 1 An illustration of Vietoris–Rips filtration with varying scales ϵ

combinatorial objects, for example, simplicial complexes, and then the evolution of these combinatorial objects is studied as the resolution scale varies.

We start with providing a brief overview of the main relevant technical concepts.

Definition 1 (Abstract simplicial complex). Let *P* be a discrete set. Then, an abstract simplicial complex is a collection *K* of finite nonempty subsets of *P* such that if $\sigma \in K$ and $\tau \subset \sigma$, then $\tau \in K$. If $|\sigma| = k + 1$, then σ is called a k-simplex.

In case of a Euclidean space, k-simplex corresponds to a convex hull of k + 1 vertices. Hence, a 0-simplex is a vertex, a 1-simplex is an edge, a 2-simplex is a triangle, and a 3-simplex is a tetrahedron.

One of the most widely used choices for a simplicial complex within the TDA framework is a Vietoris–Rips complex which has gained its popularity due to its computational properties and tractability.

Definition 2 (Vietoris–Rips complex). Let (X, d) be a metric space, for example, \mathbb{R}^m and $P \subseteq X$ be a set of distinct points of X. Let $\epsilon > 0$ be a scale. Then the Vietoris–Rips complex $V_{\epsilon}(P)$ is an abstract simplicial complex whose finite simplices σ in P have a diameter at most ϵ , that is,

$$V_{\epsilon}(P) = \{ \sigma \subseteq P | d(u, v) \le \epsilon, \ \forall u \ne v \in \sigma \}.$$

That is, we form the *proximity graph* of P by joining two points in P whenever their pairwise distance is less than ϵ . We now consider a sequence of scales $\epsilon_1 < \epsilon_2 < \ldots < \epsilon_n$ and associated nested sequence of VR complexes called a Vietoris–Rips filtration $V_{\epsilon_1}(P) \subseteq V_{\epsilon_2}(P) \subseteq \ldots \subseteq V_{\epsilon_n}(P)$. As a result, we can study evolution of topological summaries, such as number of connected components, loops, and so forth, that appear and disappear with an increase of scale ϵ . Persistent topological features, that is, those with a longer lifespan over varying resolution $\epsilon_1 < \epsilon_2 < \ldots < \epsilon_n$ tend to be associated with the underling structural organization of the data generating process, while features with a shorter lifespan are likely to be a topological noise.

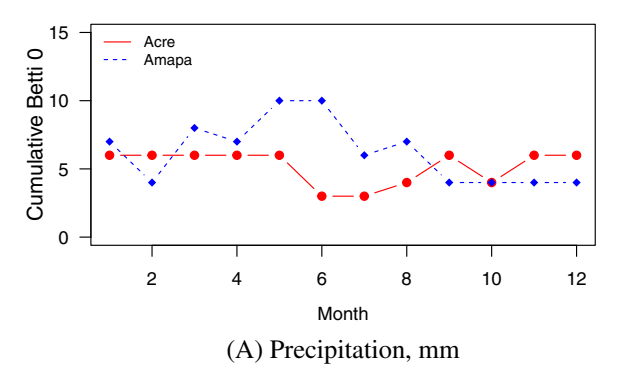
Figure 1 is an illustration of the Vietoris–Rips filtration process based on a toy example of six points. The filtration starts with a ball of radius 0 (ϵ = 0) around each point (see Figure 1a). As the scale ϵ increases to 0.2, 0.5, and 1 (see Figure 1b–d, respectively), the number of connected components decreases and new topological features, such as the loop, appear.

There exist multiple topological summaries to quantify evolution of topological features over the increasing scale ϵ , for example, barcode, persistent diagrams, persistent landscapes, and Betti numbers (see the discussion in Chazal & Michel, 2017, and references therein). In this project we focus on utility analysis of Betti numbers.

Definition 3 (Betti number). The Betti-k number β_k is the rank of the kth homology group. That is, $\beta_k(\epsilon)$ is the number of k-dimensional simplicial complex features for a given scale ϵ .

For a given scale ϵ and a given abstract simplicial complex, for example, the Vietoris–Rips complex, constructed from the observed point cloud under scale ϵ , Betti numbers are simply counts of particular topological features in this abstract simplicial complex. For instance, β_0 is the count of connected components in the Vietoris–Rips complex; while β_1 and β_2 are the numbers of holes and voids in the Vietoris–Rips complex, respectively.

Furthermore, we introduce the concept of *cumulative Betti numbers* which, as we find, tend to deliver more stable predictive performance for forecasting the Zika spread.



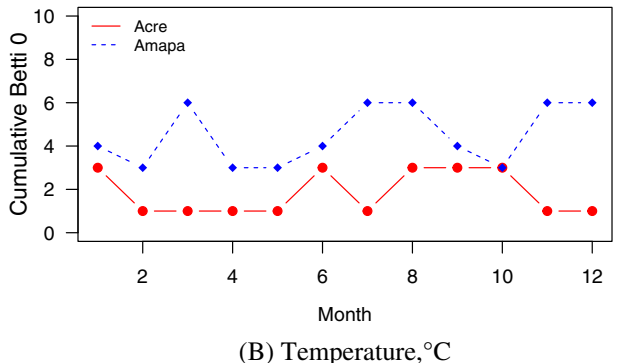


FIGURE 2 Cumulative Betti-0, $\tilde{\beta}_0$, numbers for precipitation and temperature in the states Acre and Alagoas of Brazil in 2017

Definition 4 (Cumulative Betti numbers). Over a sequence of scales $\epsilon_1 < ... < \epsilon_n$, cumulative Betti number $\tilde{\beta}_k(\epsilon_m)$, $m \le n$, is defined as the sum of Betti numbers $\beta_k(\epsilon_i)$, i = 1, ..., m. That is,

$$\tilde{\beta}_k(\epsilon_m) = \sum_{i=1}^m \beta_k(\epsilon_i), \quad m \le n.$$
(1)

In this article, due to the limited data records, we use only the $\tilde{\beta}_0$ numbers as topological descriptors, that is, the cumulative number of connected components. We hypothesize that higher predictive performance delivered by cumulative Betti numbers may be explained by higher robustness of $\tilde{\beta}_0$ to scale sequence selection under uncertainty due to low sample sizes. We used the function ripsDiag in R package TDA (Fasy et al., 2018) to find the cumulative Betti 0 numbers

Figure 2 depicts cumulative Betti-0, $\tilde{\beta}_0$, numbers based on precipitation amounts and temperature in the states of Acre and Alagoas, Brazil.

To extract the topological characteristics for precipitation $(X_{i,j}^3)$ and temperature $(X_{i,j}^4)$, we use the following algorithm. Let M_j be the number of weather stations in each state j and $X_{i,j,k}$ be the corresponding weather observations in month i $(i=1,\ldots,12;j=1,\ldots,26,$ and $k=1,\ldots,M_j)$. (Here, we suppress the superscripts for the sake of notations.) Consider a point cloud $\{X_{i,j,1},X_{i,j,2},\ldots,X_{i,j,M_j}\}$ for each month i and state j. We now measure (dis)similarity (in terms of the Euclidean distance) among recorded atmospheric variables in the ith month across all weather stations $k=1,\ldots,M_j$ in the jth state. For instance, in a case of temperature $(X_{i,j}^4)$, we set up ϵ (in degrees Celsius) and obtain a distance graph by connecting two weather stations l and l only if their recorded temperature observation differ at most l in degrees Celsius, that is, $|X_{i,j,l}-X_{i,j,m}| \le \epsilon$. We now count topological features (e.g., find the number of connected components, or Betti 0 l0 (l0) for a given scale l0. Then we increase scale l0 and repeat the procedure. Summing over the considered scales (see (1)) yields a cumulative Betti number for the l1th month in the l2th state (l1, ..., l2; l2, ..., l36). The idea is that topological summaries allow for capturing higher order dependencies among atmospheric variables that are unassessable via conventional spatio-temporal modeling approaches based on geographical proximity.

3.2 | Models

We employ three statistical and machine learning models to predict the Zika activity at the state level, namely, RF, BR, and DFFN. Using BMA, we then develop an ensemble of the Zika forecasts. We train all the models on the year 2017 data (training set), then evaluate their out-of-sample forecasts using the 2018 data (testing set). Below we provide an overview of the considered modeling approaches and the forecast validation metrics.

Let $\mathbf{Y}_{i,j}$ be the Zika rate in month i in state j ($i=1,\ldots,12$ and $j=1,\ldots,26$) and $\mathbf{X}=\{\mathbf{X}_{i,j}^1,\ldots,\mathbf{X}_{i,j}^7\}$ be the corresponding regressors. In each of the models, $\mathbf{X}_{i,j}^1$ is the precipitation, $\mathbf{X}_{i,j}^2$ is the temperature, $\mathbf{X}_{i,j}^3$ is the cumulative Betti-0 for the precipitation, $\mathbf{X}_{i,j}^4$ is the categorical variable representing month (January, ..., December), $\mathbf{X}_{i,j}^6 = \mathbf{X}_{i-1,j}^1$ is the precipitation lagged by one month, and $\mathbf{X}_{i,j}^7 = \mathbf{X}_{i-1,j}^2$ is the temperature lagged by one month. We added the lagged variables ($\mathbf{X}_{i,j}^6$ and $\mathbf{X}_{i,j}^7$) to account for delay effects.

3.2.1 | Random forest

The RF is one of the most popular models in machine learning and statistics, with an idea to combine several individual decision tree models into an additive multimodel ensemble (Breiman, 2001):

$$g(x) = \sum_{k \in \mathbb{Z}^+} f_k(x),$$

where $f_k(x)$ is an individual decision or regression tree. The two fundamental ideas behind the RF approach are (i) for constructing individual trees f_k , observations from the training set are randomly sampled with replacement (i.e., bootstrapped), and (ii) each individual split in a tree is based on a random subset of variables that are used in the model. These concepts of RF allow to reduce the effect of overfitting and to optimize a bias-variance trade-off. We used the function randomForest in R package randomForest (Breiman, Cutler, Liaw, & Wiener, 2018) to train the RF model.

3.2.2 | Generalized BR model

The generalized boosted regression model is built on two techniques: decision tree algorithms and boosting methods (Breiman, 1997; Friedman, 2001; Friedman, 2002). Generalized boosted models iteratively fit many decision trees to improve the accuracy of the model.

Let J be the number of terminal nodes in a regression tree. The tree partitions the input space X into J disjoint regions R_1, \ldots, R_J . Each regression tree model itself takes an additive form

$$h(x; \{b_j, R_j\}_1^J) = \sum_{i=1}^J b_i I(x \in R_j),$$

where b_j is the value predicted in the region R_j , x is the input datum, and $I(\cdot)$ is the indicator function. Then, the update at the mth iteration, $m \in \mathbb{Z}^+$, is

$$F_m(x) = F_{m-1}(x) + \rho_m \sum_{j=1}^J b_{jm} I(x \in R_{jm}),$$

where ρ_m is a scaling factor; $\{b_{jm}\}_{j=1}^J$ are the corresponding least-squares coefficients, and $\{R_{jm}\}_{j=1}^J$ are the regions defined by the terminal nodes of the tree at the mth iteration.

Let $\gamma_{jm} = b_{jm}\rho_m$. Note that a separate choice for optimal value γ_{jm} is proposed by Friedman (2001) in each tree region, opposed to a single γ_m in an entire tree. Update rule for model now becomes:

$$F_m(x) = F_{m-1}(x) + \sum_{j=1}^{J} \gamma_{jm} I(x \in R_{jm}), \tag{2}$$

$$\gamma_{jm} = \arg\min_{\gamma} \sum_{x_i \in R_{jm}} L(y_i, F_{m-1}(x_i) + \gamma), \tag{3}$$

where (3) is just the optimal constant update in each terminal node region, based on the loss function L, given the current approximation $F_{m-1}(x_i)$.

Additional boosting algorithm details are available in Ridgeway (2019) and Friedman (2001). For the BR, we used the function gbm in R package gbm (Greenwell, Boehmke, Cunningham, & Developers, 2019) with the number of trees equal to 100 and the interaction depth of 3, chosen through a cross-validation.

TABLE 1 Performance summary for out-of-sample forecasts in terms of MSE, MAE and Welch's *t*-test *p*-values constructed for MSEs and MAEs of the models with and without topological features

	With persistent features			Without persistent features			MSE	MAE
Method	RMSE	MAE	$r(y,\hat{y})$	RMSE	MAE	$r(y,\hat{y})$	<i>p</i> -value	<i>p</i> -value
Random forest	11.351	8.262	0.391	12.134	8.667	0.307	0.348	0.396
Boosted regression	13.238	9.154	0.363	15.044	10.091	0.286	0.093	0.262
DFFN	8.934	6.361	0.425	10.953	8.084	0.347	0.001	0.007
BMA-RMSE	6.721	4.265	0.419	8.380	7.854	0.397	< 0.001	< 0.002

Abbreviations: BMA, Bayesian model averaging; DFFN, deep feed-forward neural network; MAE, mean absolute error; RMSE, root mean square error.

TABLE 2 Welch's *t*-test *p*-values for comparison of predictive gains delivered by the deep feed-forward network vs. random forest and boosted regression

Model	With persistent features	Without persistent features
Random forest	0.002	0.277
Boosted regression	< 0.001	0.203

3.2.3 Deep feed-forward neural network

The DFFN algorithm (Hagan & Menhaj, 1994; Riedmiller & Braun, 1993; Zhang, Zhang, Lok, & Lyu, 2007) is performed as follows: input data move forward from input to hidden layers to output, and at each of those moves the data are nonlinearly transformed (using so-called *activation function*) and reweighted. When reaching the output layer, the error is calculated, based on a selected cost function, which reflects how far the DFFN output is with respect to the actual data (i.e., Zika rate) in the training set.

To illustrate the DFFN algorithm, let w_{jk}^l be the weight connecting the kth neuron in the (l-1)th layer to the jth neuron in the lth layer, and let $\sigma(\cdot)$ be the activation function (we use sigmoid function), where $j, k, l \in \mathbb{Z}^+$. The activation values at each layer are calculated in the forward procedure as

$$a_j^l = \sigma \left(\sum_k w_{jk}^l a_k^{l-1} + b_j^l \right),$$

where b_j^l is the bias coefficient, analogous to the intercept term in regression models. After calculating the total error at the output layer, a partial derivative of the cost function with respect to each weight and bias term is obtained. We train DFFN using h20.deeplearning function in R package h20 (LeDell et al., 2019). The optimal structure for DFFN is selected through a cross-validation: with two hidden layers, 12 nodes in each layer, and learning rate 0.01.

3.2.4 | Bayesian model averaging

We evaluate uncertainty of epidemiological forecasts by constructing a weighted multimodel ensemble. This application of BMA enables a combination of multiple models, with their respective weights assigned according to the models' most recent predictive performance (Fragoso, Bertoli, & Louzada, 2018; Hoeting, Madigan, Raftery, & Volinsky, 1999; Raftery, Gneiting, Balabdaoui, & Polakowski, 2005).

In this project, we define model weights within a BMA using root mean square error (RMSE) calculated for the training set of data:

RMSE(s) =
$$\sqrt{\frac{\sum_{i=1}^{12} \sum_{j=1}^{26} (y_{ij} - \tilde{y}_{ij}(s))^2}{n}}$$
,

where y_{ij} is the observed data point (in our case, the observed Zika rate in *i*th month of 2017 at the *j*th state), $\tilde{y}_{ij}(s)$ is the corresponding estimate delivered by the *s*th model (s = 1, ..., S), n is the total size of the training dataset, and S is the number of models. Then, the resulting weight ω_s for the *s*th model in the BMA ensemble of forecasts is computed as

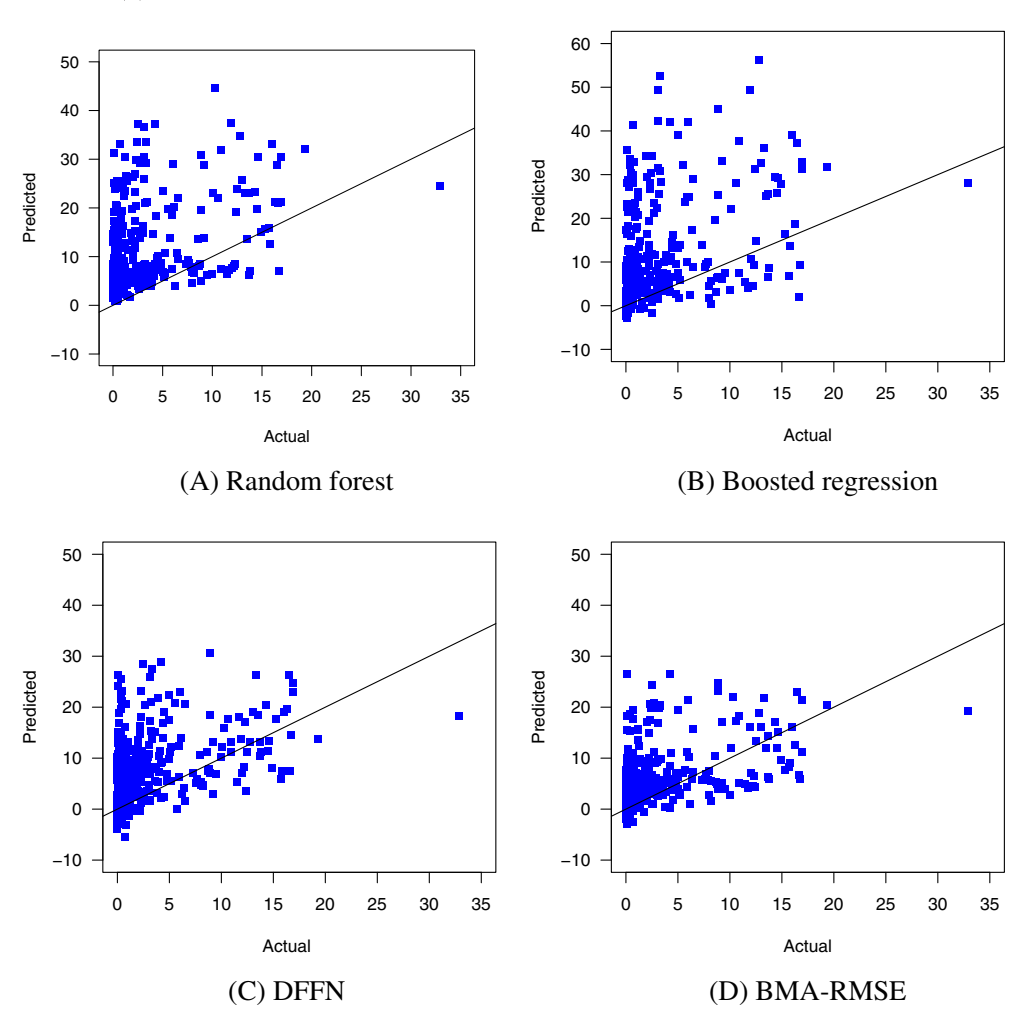


FIGURE 3 Predicted values from each of the four models vs. the actual Zika rate in 2018. The black 45° lines represent the case of ideal prediction accuracy

follows:

$$\omega_s = \frac{1/\text{RMSE}(s)}{\sum_{i=1}^{S} 1/\text{RMSE}(i)}.$$

Now, let Pred(s) (s = 1, ..., S) denote an out-of-sample forecast produced by the sth model (in our case, the Zika rate forecast of the sth model for the jth state and ith month in 2018). Then the multimodel BMA forecast for that state is defined as

$$\operatorname{Pred}_{\operatorname{RMSE}} = \sum_{s=1}^{S} \omega_{s} \operatorname{Pred}(s).$$

We set s = 1 to represent the RF model, s = 2 to represent generalized BR, and s = 3 to correspond to the DFFN.

3.3 | Validation metrics

We employ two standard statistical measures of accuracy, that is, RSME and mean absolute error (MAE) (Bluman, 2009; Kim & Ahn, 2019; Peck, Olsen, & Devore, 2015). Let $y_{i,j}$ and $\hat{y}_{i,j}$ be the observed and predicted Zika rates for the *i*th month in *j*th state in the testing dataset. Then,

RMSE =
$$\sqrt{\frac{\sum_{i=1}^{12} \sum_{j=1}^{26} (\hat{y}_{i,j} - y_{i,j})^2}{N}}$$
,

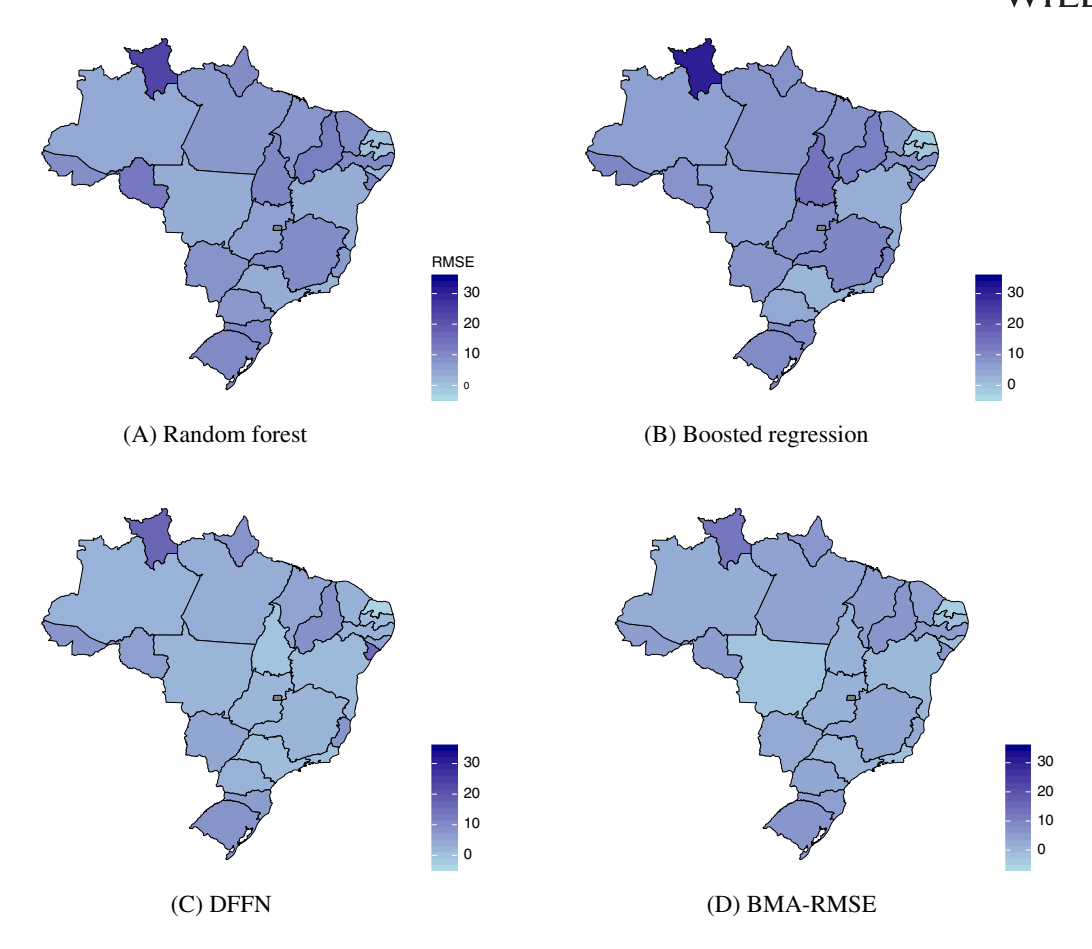


FIGURE 4 Map of predictive root mean square error (RMSE) in Brazil delivered by each of the four models for Zika rate in 2018

MAE =
$$\frac{1}{N} \sum_{i=1}^{12} \sum_{j=1}^{26} |\hat{y}_{i,j} - y_{i,j}|$$
,

where N is the size of the testing dataset. In addition, correlation between observed and forecasted values is measured through the Pearson correlation coefficient

$$r(y,\hat{y}) = \frac{\sum_{i=1}^{12} \sum_{j=1}^{26} (\hat{y}_{i,j} - \overline{\hat{y}})(y_{i,j} - \overline{y})}{\sqrt{\sum_{i=1}^{12} \sum_{j=1}^{26} (\hat{y}_{i,j} - \overline{\hat{y}})^2} \sqrt{\sum_{i=1}^{12} \sum_{j=1}^{26} (y_{i,j} - \overline{y})^2}},$$

where \bar{y} denotes average Zika rate across all states of Brazil in year 2018, and \hat{y} is the average of out-of-sample predictions across all the states for the corresponding period.

Lower RMSE, MAE, and higher Pearson correlation coefficient imply better forecasting performance.

4 | RESULTS

We train our models based on the data observed in the year of 2017 and use the 2018 data for verification. In particular, let $\mathbf{Y}_{i,j}$ be a vector of Zika rates in the *i*th month and the *j*th state of year 2017, and let \mathbf{X} be a matrix of regressors (i.e., design matrix) in the year of 2017. We now compare the performance of the models with persistent features (i.e., with the full set of inputs $X_{i,j}^1, \dots, X_{i,j}^7$) against the models without persistent features (i.e., including only $X_{i,j}^1, X_{i,j}^2$, and $X_{i,j}^5$ as the

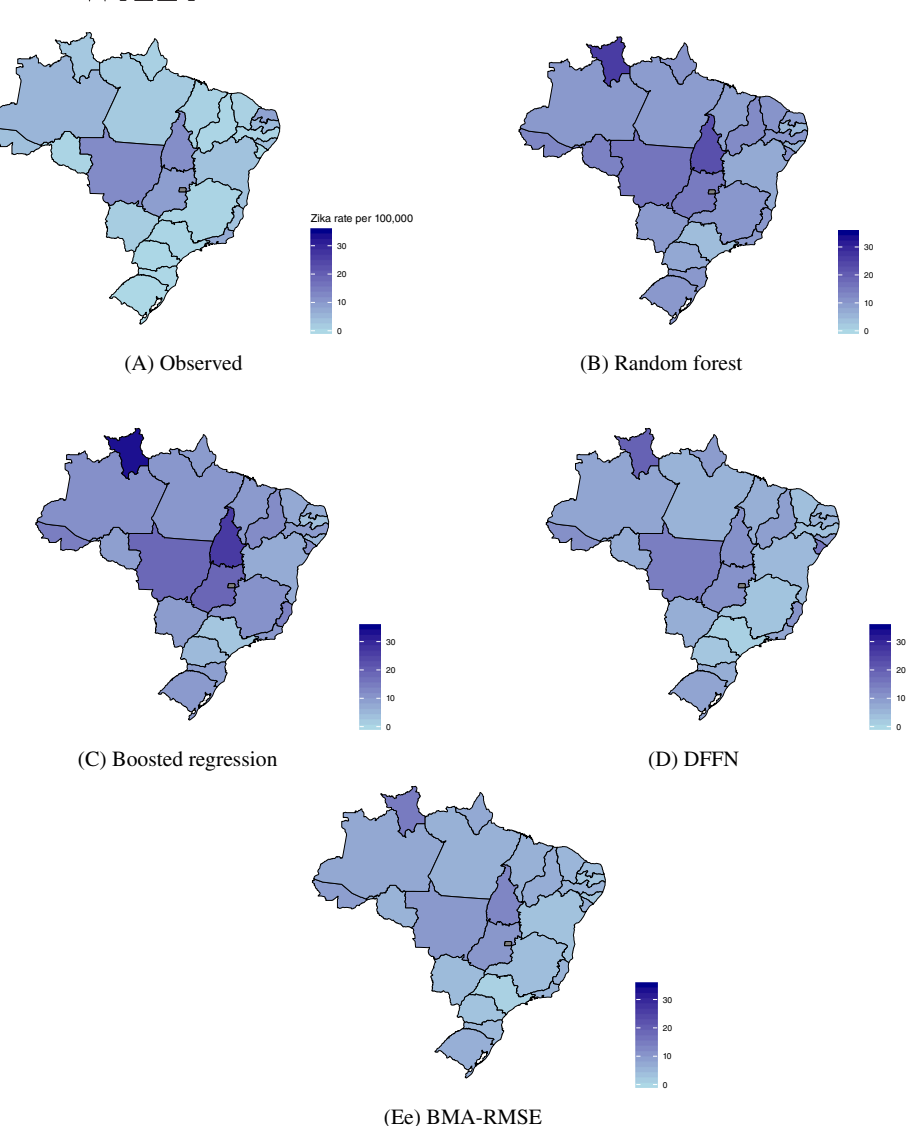


FIGURE 5 Map of the (a) observed average Zika rate in 2018 and (b–e) average predicted Zika rates in 2018 by each of the four models

inputs). As Table 1 demonstrates, models with persistent features tend to perform better than models without persistent features.

To address whether predictive power of models with topological features is significantly different from models without topological features, we perform Welch's *t*-test (Starnes, Yates, & Moore, 2010; Welch, 1947) on the absolute and squared errors delivered by models with and without topological predictors, under the null hypothesis that topological predictors yield no predictive gain. In addition, we assess whether the deep learning model (i.e., a deep feed-forward network) yields a significantly different predictive gain comparing to RF and BR.

Table 1 indicates that topological features lead to a highly statistically significant predictive gain, while incorporated into the DL DFFN model. However, while topological features result in lower predictive RMSEs for RF and BR, the predictive gains evaluated using Welch's t-test, appear to be not significant. In turn, Table 2 suggests that DFFN with persistent features delivers the most competitive predictive performance among the three individual models, with Welch's t-test p-values of < 0.001.

As expected, given the DFFN competitiveness, the BMA forecasting results are largely driven by the performance dynamics of DFFN and as such, topological descriptors are found to deliver highly statistically significant forecasting utility within the BMA framework (see Table 1).

For example, the incorporation of the persistent features lowers the RMSE of RF by 6.5%, BR by 12.0%, and DFFN by 18.4%, while the RMSE of the BMA decreases by 19.8%. Similar improvements are observed in terms of MAE, with the MAE of BMA decreasing by 45.7%.

Among the three individual models considered in this study, the tree-based models deliver the lowest forecasting performance. Figure 3a shows the RF predictions are grouped above the 45-degree line, denoting over-prediction of the Zika rates; bias of RF is a well-known issue (see technical details, e.g., in chapter 15 by Hastie, Tibshirani, & Friedman, 2009). The predictions from other models are less biased overall. Particularly, DFFN (Figure 3c) and BMA (Figure 3d) show a better balance of over-prediction and under-prediction. However, the individual errors are larger (points in the graphs for BR are farther from the 45-degree line) than for RF, see Figure 3b.

In addition, we examine the geographical distribution of prediction errors of each model. The map in Figure 4 suggests that the BMA–RMSE approach delivers the highest predictive performance for all considered states. Remarkably, among the best predicted states using the BMA–RMSE approach are the states with the highest infection rates, that is, Mato Grosso, Goias, and Mato Grosso do Sul (see also Figure 5 showing the average Zika rates and Ragas, 2018).

Remark 1. Finally, while Pearson correlations reported in Table 1 are generally low, the resulting correlations appear to be overall on par with the previous studies on Zika in other Latin and Southern American countries (McGough et al., 2017). In particular, McGough et al. (2017) report Pearson correlations for 3-week ahead forecast of Zika in Honduras not exceeding 0.35 and as low as 0.08. Similar magnitude of Pearson correlations of about 0.30 are found for autoregressive models for 3-week ahead forecast in Colombia, while correlations in El Salvador, Martinique, and Venezuela tend to be somewhat higher. Overall, correlations reported by McGough et al. (2017) tend to vary substantially among countries and among predictive models and to decrease noticeably with the increase of the forecasting horizon.

5 | DISCUSSION

Zika continues to be one of the primary healthcare concerns in the Americas, Oceania, Africa and many other parts of the world—making the virus a global challenge for healthcare professional worldwide and demanding the world's collective preparedness for this climate-sensitive (re)emerging disease.

In this article, we have brought the concepts of TDA of atmospheric variables to enhance prediction of Zika virus. In particular, we have integrated the cumulative Betti numbers as topological descriptors of precipitation and temperature dynamics—one of the key environmental factors in Zika spread—into three predictive machine learning models for Zika: RF, BR, and DFFN. To better account for various sources of uncertainties and harness the power of individual predictive models, we have combined the resulting individual forecasts into an ensemble of the Zika spread predictions using BMA. Our findings based on the analysis of Zika space-time spread in Brazil have indicated that topological summaries of precipitation dynamics and air temperature contain important predictive information for the future Zika spread.

In the future we plan to advance the proposed topological approach to analysis of other related climate-sensitive diseases such as chikungunya and dengue, in Brazil and other countries. Furthermore, epidemiological forecasting can benefit from using the tools of TDA for understanding the spread of diseases through examination of the joint dynamics of topological summaries of the disease rates and associated environmental and socioeconomic factors.

Finally, there also exist multiple directions how to better account for various types of uncertainties associated with biosurveillance of emerging climate-sensitive infectious diseases. To address the issue of limited data records and noisy epidemiological information, we plan to integrate various nontraditional data sources, such as web queries, into surveillance and forecasting of the emerging infectious diseases. Understanding topological summaries of such nontraditional data sources and matching topological patterns of the conventional data from public health units and web queries can shed a light on future spatial dynamics of the emerging infectious disease. We then plan to employ the semiparametric bootstrap to develop probabilistic forecasts associated with each model and multiple data sources, which in return can be combined into a joint biosurveillance ensemble.

ACKNOWLEDGEMENTS

Yulia R. Gel has been support in part by the grant NSF DMS 1925346.

REFERENCES

Bluman, A. G. (2009). Elementary statistics: A step by step approach. New York, NY: McGraw-Hill Higher Education.

Breiman, L. (1997). Arcing the edge. Technical Report 486. Berkeley, CA: Statistics Department, University of California.

Breiman, L. (2001). Random forests. Machine Learning, 45(1), 5–32.

Breiman L, Cutler A, Liaw A, Wiener M, 2018. Randomforest: Breiman and Cutler's random forests for classification and regression. R package version 4.6-14.

- Caminade, C., Turner, J., Metelmann, S., Hesson, J. C., WMSC, B., Solomon, T., ... Baylis, M. (2017). Global risk model for vector-borne transmission of Zika virus reveals the role of El Niño 2015. *Proceedings of the National Academy of Sciences*, 114(1), 119–124.
- Carlsson, G. (2009). Topology and data. Bulletin of the American Mathematical Society, 46(2), 255-308.
- Castro, M. C., Han, Q. C., Carvalho, L. R., Victora, C. G., & França, G. V. (2018). Implications of Zika virus and congenital Zika syndrome for the number of live births in Brazil. *Proceedings of the National Academy of Sciences*, 115(24), 6177–6182.
- CDC 2018. Centers for disease control and prevention (About Zika).
- Chazal F, Michel B, 2017. An introduction to topological data analysis: Fundamental and practical aspects for data scientists. arXiv Preprint arXiv:1710.04019.
- Costa JP, Škraba P, 2014. A topological data analysis approach to epidemiology. Paper presented at: Proceedings of the European Conference of Complexity Science.
- Dick, G. (1952). Zika virus (II): Pathogenicity and physical properties. *Transactions of the Royal Society of Tropical Medicine and Hygiene*, 46(5), 521–534.
- Dick, G., Kitchen, S., & Haddow, A. (1952). Zika virus (I): Isolations and serological specificity. *Transactions of the Royal Society of Tropical Medicine and Hygiene*, 46(5), 509–520.
- Diggle, P., Rowlingson, B., & Tl, S. (2005). Point process methodology for on-line spatio-temporal disease surveillance. *Environmetrics*, 16(5), 423–434.
- Fasy BT, Kim J, Lecci F, Maria C, Millman DL, Rouvreau V, Morozov D, Bauer U, Kerber M, Reininghaus J, 2018. TDA: Statistical tools for topological data analysis. R Package Version 1.6.4.
- Ferraris, P., Yssel, H., & Missé, D. (2019). Zika virus infection: An update. Microbes & Infection, 21(8-9), 353-360.
- Fragoso, T. M., Bertoli, W., & Louzada, F. (2018). Bayesian model averaging: A systematic review and conceptual classification. *International Statistical Review*, 86(1), 1–28.
- Friedman, J. H. (2001). Greedy function approximation: A gradient boosting machine. Annals of Statistics, 29(5), 1189-1232.
- Friedman, J. H. (2002). Stochastic gradient boosting. Computational Statistics & Data Analysis, 38(4), 367–378.
- Gidea, M., & Katz, Y. (2018). Topological data analysis of financial time series: Landscapes of crashes. *Physica A: Statistical Mechanics and Its Applications*, 491, 820–834.
- Goeijenbier, M., Slobbe, L., Van der Eijk, A., de Mendonça, M. M., Koopmans, M., & Reusken, C. (2016). Zika virus and the current outbreak: An overview. *The Netherlands Journal of Medicine*, 74(3), 104–109.
- Greenwell B, Boehmke B, Cunningham J, Developers G, 2019. GBM: Generalized Boosted Regression Models. R package version 2.1.5.
- Hagan, M. T., & Menhaj, M. B. (1994). Training feedforward networks with the Marquardt algorithm. *IEEE Transactions on Neural Networks*, 5(6), 989–993.
- Hastie, T. J., Tibshirani, R. J., & Friedman, J. H. (2009). The elements of statistical learning: data mining, inference, and prediction (2nd ed.). New York, NY: Springer.
- Heukelbach, J., Alencar, C. H., Kelvin, A. A., de Oliveira, W. K., & de Góes Cavalcanti, L. P. (2016). Zika virus outbreak in Brazil. *The Journal of Infection in Developing Countries*, 10(02), 116–120.
- Hoeting, J. A., Madigan, D., Raftery, A. E., & Volinsky, C. T. (1999). Bayesian model averaging: A tutorial. Statistical Science, 14(4), 382-401.
- INMET, 2019. Instituto nacional de meteorologia. Retrieved from http://www.inmet.gov.br/portal/index.php?r=home2/index.
- Islambekov, U., & Gel, Y. R. (2019). Unsupervised space-time clustering using persistent homology. Environmetrics, 30(4), e2539.
- Islambekov, U., Yuvaraj, M., & Gel, Y. R. (2019). Harnessing the power of topological data analysis to detect change points. *Environmetrics*, 31(1), e2612.
- Jang, M. J., Lee, Y., Lawson, A. B., & Browne, W. J. (2007). A comparison of the hierarchical likelihood and Bayesian approaches to spatial epidemiological modelling. *Environmetrics*, 18(7), 809–821.
- Kim, J., & Ahn, I. (2019). Weekly ILI patient ratio change prediction using news articles with support vector machine. *BMC Bioinformatics*, 20(1), 259.
- LeDell E, Gill N, Aiello S, Fu A, Candel A, Click C, Kraljevic T, Nykodym T, Aboyoun P, Kurka M, Malohlava M, 2019. H₂O: R Interface for 'H₂O'. R package version 3.26.0.2.
- Li, B., Ofori-Boateng, D., Gel, Y. R., & Zhang, J. (2020). A hybrid approach for transmission grid resilience assessment using reliability metrics and power system local network topology. *Sustainable and Resilient Infrastructure*, 1–16. https://doi.org/10.1080/23789689.2019.1708182.
- Lo, D., & Park, B. (2018). Modeling the spread of the Zika virus using topological data analysis. PloS One, 13(2), e0192120.
- Loh, J. M. (2011). K-scan for anomaly detection in disease surveillance. *Environmetrics*, 22(2), 179–191.
- Malone, R. W., Homan, J., Callahan, M. V., Glasspool-Malone, J., Damodaran, L., Schneider, A. D. B., et al. (2016). Zika virus: Medical countermeasure development challenges. *PLoS Neglected Tropical Diseases*, 10(3), e0004530.
- Manore C, Hyman M, 2016. Mathematical models for fighting Zika virus. Siam News.
- McDermott, P. L., & Wikle, C. K. (2019). Deep echo state networks with uncertainty quantification for spatio-temporal forecasting. *Environmetrics*, 30(3), e2553.
- McGough, S. F., Brownstein, J. S., Hawkins, J. B., & Santillana, M. (2017). Forecasting Zika incidence in the 2016 Latin America outbreak combining traditional disease surveillance with search, social media, and news report data. *PLoS Neglected Tropical Diseases*, 11(1), e0005295.
- MHB 2018. Ministry of health of Brazil; Retrieved from http://portalms.saude.gov.br/boletins-epidemiologicos.
- Muñoz, Á. G., Thomson, M. C., Stewart-Ibarra, A. M., Vecchi, G. A., Chourio, X., Nájera, P., ... Yang, X. (2017). Could the recent Zika epidemic have been predicted? *Frontiers in Microbiology*, 8, 1291.

- Nobre, A. A., Schmidt, A. M., & Lopes, H. F. (2005). Spatio-temporal models for mapping the incidence of malaria in Pará. *Environmetrics*, 16(3), 291–304.
- Peck, R., Olsen, C., & Devore, J. L. (2015). Introduction to statistics and data analysis. Boston, MA: Cengage Learning.
- Raftery, A. E., Gneiting, T., Balabdaoui, F., & Polakowski, M. (2005). Using Bayesian model averaging to calibrate forecast ensembles. *Monthly Weather Review*, 133(5), 1155–1174.
- Ragas, J. (2018). Revisiting global health from the periphery: The Zika virus. História, Ciências, Saúde-Manguinhos, 25(4), 1185-1187.
- Rees, E. E., Petukhova, T., Mascarenhas, M., Pelcat, Y., & Ogden, N. H. (2018). Environmental and social determinants of population vulnerability to Zika virus emergence at the local scale. *Parasites & Vectors*, 11(1), 290.
- Ridgeway, G. (2019). Generalized boosted models: A guide to the GBM package. Update, 1(1), 2019.
- Riedmiller M, Braun H, 1993. A direct adaptive method for faster backpropagation learning: The RPROP algorithm. Paper presented at: Proceedings of the IEEE International Conference on Neural Networks, volume 1993, 586–591. San Francisco, CA.
- Saggar, M., Sporns, O., Gonzalez-Castillo, J., Bandettini, P. A., Carlsson, G., Glover, G., & Reiss, A. L. (2018). Towards a new approach to reveal dynamical organization of the brain using topological data analysis. *Nature Communications*, 9(1), 1399.
- Self, S. C. W., McMahan, C. S., Brown, D. A., Lund, R. B., Gettings, J. R., & Yabsley, M. J. (2018). A large-scale spatio-temporal binomial regression model for estimating seroprevalence trends. *Environmetrics*, 29(8), e2538.
- Seo J, Lee J, Kim K, 2018. Decoding of polar code by using deep feed-forward neural networks. Paper presented at: Proceedings of the 2018 International Conference on Computing, Networking and Communications (ICNC), 238–242. IEEE.
- Soliman, M., Lyubchich, V., & Gel, Y. R. (2019). Complementing the power of deep learning with statistical model fusion: Probabilistic forecasting of influenza in Dallas County, Texas. *Epidemics*, 28, 100345.
- Starnes, D. S., Yates, D., & Moore, D. S. (2010). The practice of statistics. New York, NY: Palgrave Macmillan.
- Suparit, P., Wiratsudakul, A., & Modchang, C. (2018). A mathematical model for Zika virus transmission dynamics with a time-dependent mosquito biting rate. *Theoretical Biology and Medical Modelling*, 15(1), 11.
- Teng, Y., Bi, D., Xie, G., Jin, Y., Huang, Y., Lin, B., ... Tong, Y. (2017). Dynamic forecasting of Zika epidemics using Google trends. *PloS One*, 12(1), e0165085.
- Tjaden, N. B., Thomas, S. M., Fischer, D., & Beierkuhnlein, C. (2013). Extrinsic incubation period of dengue: Knowledge, backlog, and applications of temperature dependence. *PLoS Neglected Tropical Diseases*, 7(6), e2207.
- Torabi, M. (2013). Spatio-temporal modeling for disease mapping using car and b-spline smoothing. Environmetrics, 24(3), 180-188.
- Ugarte, M., Goicoa, T., Ibanez, B., & Militino, A. (2009). Evaluating the performance of spatio-temporal Bayesian models in disease mapping. *Environmetrics*, 20(6), 647–665.
- Welch, B. L. (1947). The generalization of student's problem when several different population variances are involved. *Biometrika*, 34(1/2), 28–35.
- WHO, 2019. World Health Organization. Retrieved from http://www.who.int/emergencies/diseases/zika/en/.
- World-Weather-Online, 2018. Retrieved from www.worldweatheronline.com/.
- Zhang, J. R., Zhang, J., Lok, T. M., & Lyu, M. R. (2007). A hybrid particle swarm optimization–back-propagation algorithm for feedforward neural network training. *Applied Mathematics and Computation*, 185(2), 1026–1037.
- Zomorodian, A., & Carlsson, G. (2005). Computing persistent homology. Discrete & Computational Geometry, 33(2), 249–274.

How to cite this article: Soliman M, Lyubchich V, Gel YR. Ensemble forecasting of the Zika space-time spread with topological data analysis. *Environmetrics*. 2020;1–13. https://doi.org/10.1002/env.2629